Acta Cryst. (1999). A**55**, 803–810

Structure of the alloy $Ti_{50}Ni_{48.7}Co_{1.3}$

Z. Lekston,[a] V. E. Naish,[b] T. V. Novoselova[b]* and I. V. Sagaradze[b]

[a]*Institute of Physics and Chemistry of Metals, University of Silesia, Katowice, Poland, and* [b]*Institute for Metal Physics, str. S. Kovalevskaya 18, 620219 Ekaterinburg, Russia. E-mail: tatiana.novoselova@imp.uran.ru*

(*Received 23 June 1998; accepted 27 January 1999*)

Abstract

The structure of the *R* phase of the alloy $Ti_{50}Ni_{48.7}Co_{1.3}$ was determined by the crystallogeometric analysis of martensitic transformations in titanium nickelide. This analysis is based on the concept of cooperative thermal vibrations of the (110)-like planes in the b.c.c. and *B*2 structures and their freezing (transformation to static displacements) at the point of the phase transition. The space group of the *R* phase is trigonal $P31m$ with a hexagonal Bravais lattice. The validity of the *R*-phase structure determination is confirmed by an X-ray diffraction pattern that was obtained at room temperature using Cu $K\alpha$ radiation. The Rietveld procedure was used to compare the calculated and experimental X-ray diffraction patterns. The proposed structural model of the *R* phase agrees satisfactorily with the experimental data.

1. Introduction

Determination of the crystal structures of the new phases arising from structural phase transitions often appears to be a complicated problem. On the one hand, such a problem demands experimental diffraction data that can be obtained by X-ray or neutron methods. On the other hand, it is necessary to have a model of the structure, which should be created with the help of any available physical or conceptual information. The final quantitative refinement of the structure is achieved by the use of procedures (such as Rietveld refinement) to fit the theoretical intensity profile to the experimental one. The absence (or inadequacy) of the *a priori* justification for an initial physical model of the structure is a drawback of many diffraction studies.

The situation with studies of the crystal structures of NiTi phases is an example. At high temperatures, an NiTi alloy having a nearly equiatomic composition possesses a crystal structure of the *B*2 type. At low temperatures, three martensitic phases can appear, depending on the deviation from the equiatomic stoichiometric composition, the concentration and type of dopants, the treatment of samples, and so on. They are the orthorhombic *B*19 phase, the trigonal *R* phase and the monoclinic phase. The structure of the monoclinic phase is usually considered to be a distorted *B*19 structure and is called *B*19′ (Buhrer *et al.*, 1985).

Although investigations of NiTi martensitic phases have been described in many papers, the structure of the *B*19 phase is so far the only reliably determined structure for NiTi. The situation turns out to be more intricate for the case of the *R* phase, which was considered for a long time to have a rhombohedral unit cell. That was a reason for calling this phase the '*R* phase'. Now it has been determined that the space group for the *R* phase is trigonal with a primitive hexagonal Bravais lattice. There is, however, disagreement in the literature over the choice of the actual space group. Goo & Sinclair (1985) indicated that the space group was $P\bar{3}1m$. Hara *et al.* (1995) applied the Rietveld procedure for the full-profile analysis of the diffraction pattern of a Ti–50.23 at.% Ni alloy containing the *R* phase. The space groups examined were $P311$, $P\bar{3}11$, $P31m$ and $P\bar{3}1m$. In their work, these authors have chosen space group $P311$, in spite of the common knowledge that the presence or absence of inversion symmetry cannot be determined by diffraction methods alone. The coordinates of the Ti and Ni atoms in the unit cell were also determinated by the Rietveld method. The work by Ohba *et al.* (1992), where the so-called ζ_2' phase in an Au–49.5 at.% Cd alloy which is similar to the *R* phase in NiTi is considered, may be mentioned here. The authors used the full-matrix least-squares method to determine that the ζ_2' phase had the space group $P311$ and obtained lattice parameters and atomic coordinates in the unit cell. None of these works contains any theoretical concepts or calculations that could clarify why the *B*2 lattice transforms into this trigonal structure under a martensitic phase transition.

The present work is based on the crystallogeometric theory of martensitic transformations in titanium nickelide developed earlier (Naish *et al.*, 1995, 1997). This theory allows an independent (of experiment) analysis of the structures of possible martensitic phases with a theoretical determination of their space groups, lattice parameters and the atomic coordinates. To test the theoretical results, we obtained X-ray powder diffraction patterns for an alloy with the composition $Ti_{50}Ni_{48.7}Co_{1.3}$ in the *R* phase. All the structure parameters calculated by the theory were refined by a

ISSN 0108-7673

comparison of theoretical and measured peak positions, as well as relative intensities for X-ray reflections. Finally, we have compared our results with the experimental data of Hara *et al.* (1995) and of Shapiro (1981), and have obtained satisfactory agreement.

2. The cooperative thermal vibrations concept

Crystallogeometrical analysis of martensitic transformations in titanium nickelide and of structural phase transitions in many other crystals constructed using the concept of cooperative thermal vibrations and their transformation into static displacements has been developed in our previous papers. The results of these studies were reviewed by Kassan-Ogly *et al.* (1994).

The concept of cooperative thermal vibrations is based on the hypothesis that there exist atomic chains or atomic planes (one- or two-dimensional objects) in which the atomic vibrations are correlated, so that coherent structural relationships within the objects are retained. The existence of such vibrations is easily confirmed by the pictures of sharp anisotropic thermal diffuse scattering of X-rays and electrons in the so-called mono-Laue scheme (fixed beam–fixed crystal). A detailed discussion of such experiments is contained in the review by Kassan-Ogly *et al.* (1994). In the majority of cases, the crystallogeometrical analysis of a structure furnishes a determination of the objects in the structure *a priori*. The *B*2 structure, which is found in NiTi at high temperatures, is an example. The coherent objects are the (110) atomic planes, which are only capable of moving within their own planes along the $[1\bar{1}0]$ directions. Mono-Laue diffraction patterns (Naish *et al.*, 1995) confirm this conclusion.

At the phase-transition point, the vibrations of extended coherent objects become frozen, transforming into static displacements. The response of a distorted crystal to these displacements is densification (or contraction), which can be regarded as a uniform strain. As a result, the parent structure can be transformed, leading to a structural phase transition of a cooperative (martensite) type, because the displacements and vibrations of atoms are correlated.

The initial high-symmetry phase possesses several crystallographically equivalent families of extended objects so that the structure of the new phase depends on the number of object families participating simultaneously in the process of freezing. It is convenient to describe the set of freezing families in terms of the multicomponent order parameter

$$\eta = \sum C_i \eta_i, \tag{1}$$

where each component η_i corresponds to one family, and the set of nonzero mixing coefficients $\{C_i\}$ determines the variant of simultaneous freezing of cooperative vibrations. From the physical viewpoint, it is reasonable to consider only the high-symmetry variants of mixing in the space of the order parameter. Other variants have unfavorable energies.

3. Configurations of static displacements within one family

Except for variants of mixing, the structure of the martensitic phase depends on configurations of static displacements of the extended objects within each family that is present after freezing. In our case, these are the configurations of the displacements of parallel and equidistant (110)-type planes along themselves. It is convenient to describe these configurations by a wave-vector of the configuration, **q**. Here we are dealing with an essentially one-dimensional sequence of parallel planes numbered 0, 1, 2, ..., n, ... with interplanar spacing d. Thus, we may use a one-dimensional wave-vector q.

Let us assume that the configuration of plane displacements is periodic with a period t. The wave-vector q specifies the value of t but it says nothing about the mutual displacements within one period. In what follows, all distances in real space are stated as fractions of d, while those in reciprocal space are stated as fractions of $2\pi/d$. The displacement Δ_n of plane n can be obtained from the displacement Δ_0 of the initial plane by the equation

$$\Delta_n = \Delta_0 \exp(2\pi i q n). \tag{2}$$

For $q = 1/2$, where the period is $t = 2$, we have $\Delta_0 = \Delta_2 = \Delta_4 = \ldots$. For $q = 1/3$, the period is $t = 3$, and so on.

It makes no sense to consider the configurations with a very small q (large period t), so we (Naish *et al.*, 1997) have only analyzed the cases with periods $t = 1, 2, 3$ and 4, corresponding to $q = 0$, $1/2$, $1/3$ and $1/4$. The theoretical basis for the choice of configurations of the families of static plane displacements is a set of the eigenstates of the one-dimensional Ising Hamiltonian.

For the Ising model, we use the Ising operator $\sigma_n = \pm 1$, which can be assigned either to the plane numbered n or to the space between the $(n-1)$th and nth planes. In their turn, values $\sigma = +1$ and -1 express either the absolute plane displacement or the displacement with respect to the adjacent planes (the relative displacements). The Ising Hamiltonian can be written in the nearest-neighbor approximation as

$$H = -V \sum \sigma_n \sigma_{n+1}, \tag{3}$$

or the next-nearest-neighbor approximation

$$H = -V \sum \sigma_n \sigma_{n+1} - V' \sum \sigma_n \sigma_{n+2}. \tag{4}$$

Approximation (3) is sufficient to describe the configurations of the static displacements with periods $t = 0$ and 1. In this case, the ground eigenstates are the following Ising configurations:

$$V > 0: \quad \sigma_1 = \sigma_2 = \sigma_3 = \ldots \quad \text{'ferromagnetic'}; \quad t = 1,\ q = 0;$$
$$V < 0: \quad \sigma_1 = -\sigma_2 = \sigma_3 = -\sigma_4 \quad \text{'antiferromagnetic'}; \quad t = 2,\ q = 1/2. \qquad (5)$$

The 'ferromagnetic' Ising configuration has no physical sense for the description of the absolute displacements because this case describes movement of the crystal as a whole. For relative displacements, the 'ferromagnetic' Ising configuration corresponds to the configuration of static displacements represented in Fig. 1(*a*). This configuration is called the 'shear mechanism' (Naish *et al.*, 1995, 1997; Kassan-Ogly *et al.*, 1994) and it means that the displacement of each plane with respect to the previous one leads to the accumulation of the total macroscopic shear.

The 'antiferromagnetic' configuration, in terms of both absolute and relative displacements, describes the situation in which the plane displacements are compensated at each successive interplanar spacing. This configuration is represented in Fig. 1(*b*) and is called 'the compensation mechanism' (Naish *et al.*, 1995, 1997; Kassan-Ogly *et al.*, 1994).

To describe the more complicated configurations of static displacements with periods $t = 3$ or 4, it is necessary to analyze the Hamiltonian (4). Its eigenstates depend on the signs of parameters V and V' and the relation $s = |V/V'|$. This problem was considered in detail in the work of Kassan-Ogly *et al.* (1989) and of Grebennikov & Naish (1991).

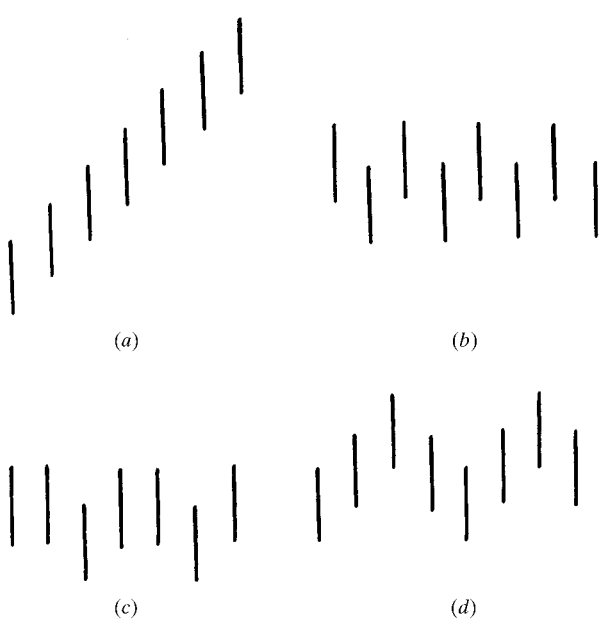

Fig. 1. Types of configuration of the relative displacements of (110)-type planes. (*a*) Wave vector $q = 0$ (shear mechanism); (*b*) $q = 1/2$ (compensation mechanism); (*c*) $q = 1/3$; (*d*) $q = 1/4$.

For $V' > 0$ (noncompeting interactions V and V'), Hamiltonian (4), as well as Hamiltonian (3), has eigenstates (5). For $V' < 0$ (competing interactions V and V'), all results depend on the value of s. For $s > 1/4$, in addition to 'ferromagnetic' and 'antiferromagnetic' configurations, there is also an incommensurate eigenstate of Hamiltonian (4) that for s close to $1/2$ ($V < 0$, $V' < 0$) corresponds to the Ising configuration with the wavevector q close to $1/3$. This configuration cannot be the ground state and it transforms inevitably to the 'antiferromagnetic' ground state (for $s < 1/2$) or to the ground state with $q = 1/4$ (for $s > 1/2$) upon the lowering of temperature. Nevertheless, the temperature range of existence of the configuration with $q = 1/3$ is quite wide, so that this incommensurate phase may appear in real crystals. Thus, the set of configurations considered for the static displacements is extended by the configurations represented in Figs. 1(*c*) and (*d*) with $t = 3$ ($q = 1/3$) and $t = 4$ ($q = 1/4$), respectively.

In previous work (Naish *et al.*, 1997), we have considered in detail the occurrence of particular combinations of freezing configurations and mixing variants in real crystals with parent b.c.c. and *B*2 structures. In the present work, we will address the configuration in Fig. 1(*c*) with mixing variant (0*C*0*C*0*C*), which corresponds to the freezing of three plane families of types $\{\bar{1}10\}$, $\{0\bar{1}1\}$and $\{10\bar{1}\}$. These planes intersect on [111]-type lines. We show below that this case of the martensitic phase structure is the structure of the *R* phase of titanium nickelide.

4. The *R*-phase model

A crystal structure responds to the freezing of cooperative vibrations of coherent object families by densification, called 'contraction'. In b.c.c. and *B*2 structures, contraction within one family of the planes of (110) type may usefully be subdivided into intra- and interobject contraction. The intraobject contraction has two parameters, $k_{\|}$ and k_z, as is shown in Fig. 2(*a*). Interobject contraction $k_{\perp}$ 'densifies' different planes of the given family relative to one another (Fig. 2*b*). Both contraction types appear to be possible due to the mutual shifts of the planes of the family and, as a result, planes lose their interlocking relation with one another. The specific feature of the configurations of the static displacements of the coherent objects with period $t = 3$ is such that two adjacent planes with equal displacements prevent each other from interacting. Thus, contraction is impossible, and we must introduce an additional displacement p in the direction perpendicular to the planes of a chosen family. This displacement is outlined in Fig. 2(*c*), as well as the in-plane static displacements Δ. The plane passing through the zeroth atom is assumed to be immobile, the next two planes are both shifted by 2Δ, the third plane is immobile again, and so on.

The contraction-related displacements corresponding to a uniform strain can only change the lengths of the translations of the parent phase and rotate them. In contrast, the in-plane displacements 2Δ can eliminate some translations. The additional displacements p are characteristic only of the sheared planes, so they have no effect on the set of retained and lost translations.

It is clear from this analysis that the shortest non-coplanar retained translations are:

$$\mathbf{a}_1 - 2\mathbf{a}_2 + \mathbf{a}_3; \quad \mathbf{a}_1 + \mathbf{a}_2 - 2\mathbf{a}_3; \quad \mathbf{a}_1 + \mathbf{a}_2 + \mathbf{a}_3.$$

These three translations form the unit cell of the new phase. Let us denote them by $\mathbf{a}_1^H$, $\mathbf{a}_2^H$ and $\mathbf{a}_3^H$, respectively. Taking into account all atomic contraction related displacements, we can rewrite the exact components of the translations in the cubic coordinate system:

$$\begin{aligned}
\mathbf{a}_1^H &= (a + k_\parallel - 3k_\perp - 2k_z;\ -2a - 2k_\parallel + 6k_\perp + 4k_z;\\
&\quad a + k_\parallel - 3k_\perp - 2k_z);\\
\mathbf{a}_2^H &= (a + k_\parallel - 3k_\perp - 2k_z;\ a + k_\parallel - 3k_\perp - 2k_z;\\
&\quad -2a - 2k_\parallel + 6k_\perp + 4k_z);\\
\mathbf{a}_3^H &= (a + 4k_\parallel - 2k_z;\ a + 4k_\parallel - 2k_z;\ a + 4k_\parallel - 2k_z);
\end{aligned} \tag{6}$$

where a is the cubic lattice parameter of the parent $B2$ phase. It is easy to see that $(\mathbf{a}_1^H, \mathbf{a}_3^H) = (\mathbf{a}_2^H, \mathbf{a}_3^H) = 0$ so that the corresponding angles are equal to 90°. In addition, $\cos(\mathbf{a}_1^H, \mathbf{a}_2^H) = -1/2$, so that the angle between $\mathbf{a}_1^H$ and $\mathbf{a}_2^H$ is 120°. Thus, these three translations form a hexagonal unit cell. The edges of the hexagonal cell are $a^H \approx a \times 6^{1/2}$ and $c^H \approx a \times 3^{1/2}$. The exact expressions are

$$\begin{aligned}
a^H &= (a + k_\parallel - 3k_\perp - 2k_z)6^{1/2},\\
c^H &= (a + 4k_\parallel - 2k_z)3^{1/2}.
\end{aligned} \tag{7}$$

The orientation relationships between the new hexagonal cell and the parent cubic structure are

$$\begin{aligned}
&(001)_H || (111)_{B2}; \quad [100]_H || [1\bar{2}1]_{B2};\\
&[010]_H || [11\bar{2}]_{B2}; \quad [110]_H || [2\bar{1}\bar{1}]_{B2}.
\end{aligned} \tag{8}$$

The volume of the hexagonal unit cell (taking the contractions into account) is $27a^3$, *i.e.* the hexagonal cell contains 27 atoms of each type. The smallest cell (this is 1/3 of the hexagonal prism) contains 9 atoms of each type. Let us rewrite their exact coordinates (calculated by taking into account the displacements Δ, $k_\parallel$, k_z, $k_\perp$ and p) in the hexagonal coordinate system, expressed as fractions of a^H and c^H. Without loss of generality, we may assign the coordinates listed below to Ni atoms. The coordinates of the Ti atoms can be obtained from the coordinates of the Ni atoms by addition of the vector (0, 0, 1/2).

1. $0, 0, 0$
2. $1/3 - u - v, 0, 2/3 + 4\delta$
3. $0, 1/3 - u - v, 2/3 + 4\delta$
4. $2/3 + u + v, 2/3 + u + v, 2/3 + 4\delta$
5. $2/3 - u + v, 0, 1/3 + 4\delta$
6. $0, 2/3 - u + v, 1/3 + 4\delta$
7. $1/3 + u - v, 1/3 + u - v, 1/3 + 4\delta$
8. $2/3, 1/3, 6\delta$
9. $1/3, 2/3, 6\delta$.

(9)

The shifts u, v and δ are related to the displacements Δ, p, $k_\parallel$, $k_\perp$ and k_z by

$$\begin{aligned}
u &= \Delta/3(a + k_\parallel - 3k_\perp - 2k_z) = \Delta 2^{1/2}/a^H 3^{1/2},\\
v &= p/(a + k_\parallel - 3k_\perp - 2k_z) = p6^{1/2}/a^H,\\
\delta &= \Delta/3(a + 4k_\parallel - 2k_z) = \Delta/c^H 3^{1/2}
\end{aligned} \tag{10}$$

and are quantities of the order of Δ/a and p/a.

Fig. 3 depicts the structure of the unit cell. For convenience of perception, atoms are placed in their initial cubic positions. Atomic displacements from these positions are marked by the needles. Different types of

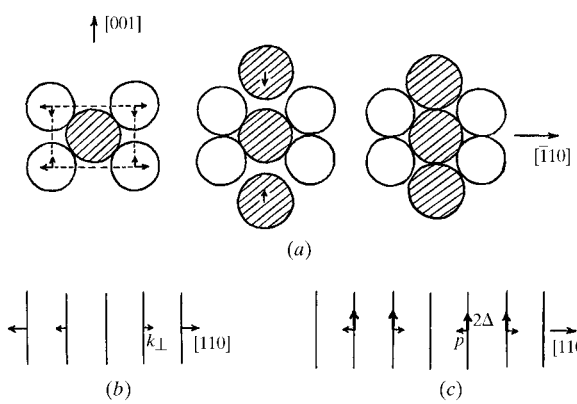

Fig. 2. (*a*) Intraobject contraction within (110) planes of the $B2$ structure in TiNi; (*b*) interobject contraction between planes; (*c*) static displacements, 2Δ, and additional displacements, p, of (110)-type planes in the configuration with $q = 1/3$.

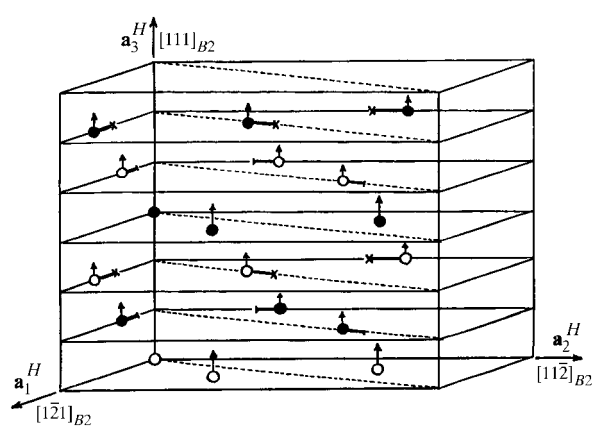

Fig. 3. The unit cell of the R phase of TiNi.

needles on the xy plane correspond to different values of the displacements ($-\circ$ means $u+v$ and $-\times$ means $u-v$). Along the z axis, the atoms of the bottom and central layers have displacements 6δ, but atoms of the other layers have displacements 4δ. Ni and Ti atoms are denoted by open and solid circles, respectively.

Fig. 4(a) illustrates the $(001)_H$ layers of the whole hexagonal prism that has three times the volume of the unit cell with all atomic displacements in the xy plane. The notation is the same as in Fig. 3. Fig. 4(a) clearly shows the existing symmetry elements: threefold symmetry axis and three mirror planes m containing the translations $\mathbf{a}_1^H$ and $\mathbf{a}_2^H$. There is no inversion center in this structure. Thus, the space group of the new phase is $C_{3v}^2 = P31m$.

As was mentioned previously, Goo & Sinclair (1985) indicated that the space group for the R phase was $P31m$, but they did not show a unit cell or give any atomic coordinates. Hara *et al.* (1995) obtained the atomic coordinates of Ni and Ti in the R phase, and Ohba *et al.* (1992), who belong to the same scientific group, obtained the coordinates of Au and Cd in the ζ_2' phase, which is similar to the R phase. In both cases, they indicated that the space group for the martensite structure is $P311$, and atoms of both types occupy all possible equivalent positions in this space group: 1(a), 1(b), 1(c) and 3(d). Fig. 1 of the unit cell from the work of Ohba *et al.* (1992) should be compared with our Fig. 3 because, first, the volume of the unit cell is one third of that of ours, as shown in Fig. 3 (in their structure, $[100]_H \| [2\bar{1}\bar{1}]_{B2}$ and $[010]_H \| [\bar{1}2\bar{1}]_{B2}$) and, second, they have not represented all atomic displacements obtained from fitting the theoretical intensity profile to the experimental one. To assist comparison, we have reproduced in Fig. 4(b) the $(001)_H$ layers of the whole hexagonal prism with the atomic displacements obtained from data of Hara *et al.* (1995) and of Ohba *et al.* (1992) for the R and ζ_2' phases. The distinction between the R and ζ_2' phases lies only in the lengths of the needles.

Our R-phase model agrees with the models of Hara *et al.* (1995) and Ohba *et al.* (1992) in size and the orientation of the parent structure with respect to the hexagonal unit cell but our model has a different space group and different atomic coordinates. Our main result consists in obtaining the R phase by an independent theoretical analysis based on the concept of cooperative thermal vibrations, without experimental data.

The values of the lattice parameters, a^H and c^H, and shifts δ, u and v can be calculated from the equations of new contacts between the atoms. From these calculations, we obtain parameters as follows:

$$a^H = 7.461\ \text{Å}, \quad c^H = 5.221\ \text{Å},$$
$$\delta = 0.055, \quad u = 0.039, \quad v = 0.017. \qquad (11)$$

Before discussing the experimental data, it is necessary to make two important comments. First, the space group of the R phase is trigonal, with a primitive hexagonal Bravais lattice. From this standpoint, the 'H phase' would be a more appropriate label than the commonly accepted 'R phase', and it seems inappropriate to speak about a rhombohedral angle as a characteristic of the R phase. It is impossible to introduce such an angle into a primitve lattice. Nevertheless, some authors keep using this label. Second, it is interesting to note that none of the published works discusses the physical meaning of the intermediate nature of the R phase. It follows from our theoretical result that this phase cannot be the ground state of titanium nickelide

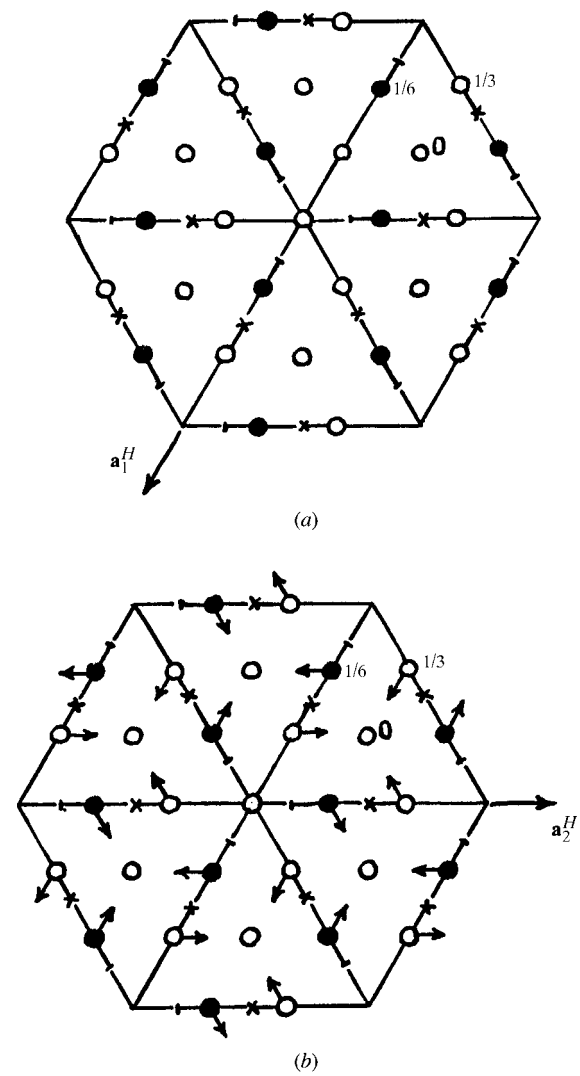

Fig. 4. $(001)_H$ layers of a hexagonal prism containing three unit cells of (a) our R-phase model of TiNi and (b) the R-phase models of Hara *et al.* (1995) and of Ohba *et al.* (1992).

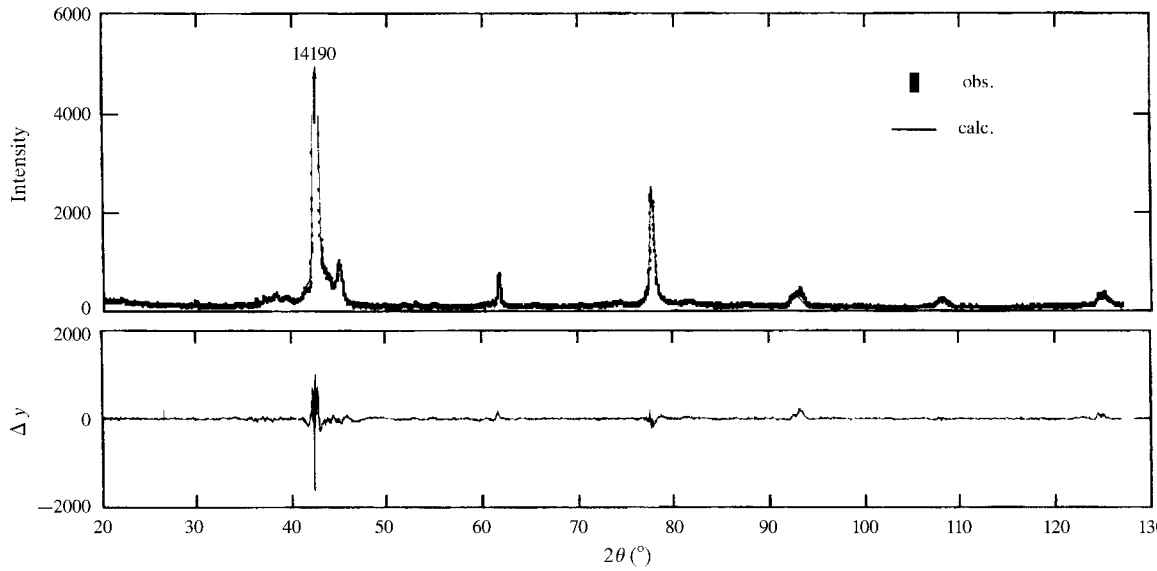

Fig. 5. Plot of observed and calculated intensities from a Rietveld refinement of X-ray powder data from the alloy $Ti_{50}Ni_{48.7}Co_{1.3}$ at room temperature.

at low temperatures. This question might be resolved by further investigation.

5. Experimental data

Most of the published structural data on the *R* phase have been obtained by electron diffraction. Only a few X-ray and neutron diffraction studies are known, and these data are not sufficient for quantitative comparison with theory. Therefore, we obtained our own X-ray diffraction pattern of the alloy $Ti_{50}Ni_{48.7}Co_{1.3}$ containing the *R* phase at room temperature.

An alloy with this nominal composition was obtained by induction melting. The ingot was homogenized under a vacuum (about 1.3×10^{-3} Pa) at 1170 K for 48 h and hot rolled to plates of thickness about 1 mm. The specimens for X-ray experiments after hot rolling were isothermally annealed at 970 K for 1 h in a resistance furnace with an argon atmosphere, then immersed in ethanol, which was cooled by dry ice to a temperature of about 210 K, and finally aged at 570 to 870 K for 1 to 9 h (Lekston, 1993).

The X-ray diffraction pattern was obtained at room temperature using a Philips X-ray diffractometer equipped with a graphite monochromator. Cu $K\alpha$ radiation was used. The diffraction pattern was recorded in the angular region from 20 to 127°(2θ) by continuous scan of the detectors with a speed of 2°(2θ) min^{-1}.†

We produced two X-ray diffraction patterns from this alloy. The first one had a strongly pronounced *R* phase at room temperature, with clear splitting of the parent *B*2 reflections and the appearance of new *R*-phase reflections. The other one was obtained from the same specimen, but after several months, so this alloy had been additionally aged at room temperature. As a result, the *R* phase is feebly marked on the diffraction pattern from it. For example, it is rather difficult to distinguish $(112)_R$ and $(300)_R$ reflections and some of the weak *R*-phase reflections are not visible on this pattern. Unfortunately, we have only compared these data with our model using Rietveld refinement (DBWS-9411) because only they have been in an appropriate form. The result is illustrated in Fig. 5. The agreement is satisfactory ($R_{\rm Bragg} = 5.86\%$; $R_p = 9.11\%$); values of adjustable parameters are

$$a^H = 7.406\,(3)\,\text{Å}, \quad c^H = 5.268\,(4)\,\text{Å},$$
$$\delta = 7.29\,(2) \times 10^{-3}, \quad u = 3.64\,(1) \times 10^{-3},$$
$$v = 1.25\,(2) \times 10^{-4}. \qquad (12)$$

6. Comparison with the literature

We have compared our *R*-phase model with diffraction data reported in the literature. The diffraction peaks of the *R* phase can be classified into three categories. The first set includes the peaks that also appear in the diffraction patterns of the parent *B*2 phase. The second set consists of reflections that also appear in the parent phase, but are split into two or even three components after the transition to the *R* phase. The third set includes the reflections that appear only in the *R* phase. These reflections can be called superstructure reflections.

† The numbered intensity of each point on the profile has been deposited with the IUCr. These data are available from the IUCr electronic archives (Reference: AU0153). Services for accessing these data are described at the back of the journal.

One of the main diffraction effects that indicates the transition to the R phase is the appearance of superstructure reflections at the so-called *type-1/3* positions along the $[110]_{B2}$, $[112]_{B2}$ and $[111]_{B2}$ directions of the initial diffraction pattern. At temperatures far above the point of the martensitic transformation, these superstructure reflections are observed as broad diffuse maxima. Their appearance is usually interpreted as one of the *pretransition phenomena*. Diffraction effects of this type were described in our recent work (Naish *et al.*, 1996) and have been observed in many other studies (see *e.g.* Khachin *et al.*, 1992). As the temperature is lowered, the widths of the diffuse maxima decrease and at the transition point they become comparable with instrumental resolution. On further cooling, the intensities of these maxima increase by two or three orders of magnitude, although they remain very weak compared to the reflections of the first and second type inherited from the $B2$ phase. Using the proposed geometrical model of the $B2 \rightarrow R$ martensitic transformation, it is easy to show that the $(100)_R$ reflection corresponds to $(1/3, -1/3, 0)_{B2}$, $(110)_R$ to $(2/3, -1/3, -1/3)_{B2}$, and $(001)_R$ to $(1/3, 1/3, 1/3)_{B2}$. Thus, the proposed model adequately describes the main diffraction phenomena.

Shapiro (1981) studied polycrystalline samples of $Ti_{50}Ni_{47}Fe_3$ at three temperatures: 300, 225 and 120 K. The last temperature falls into the existence region of the R phase. The neutron wavelength was $\lambda = 2.466$ Å. Three segments of the neutron diffraction patterns presented by Shapiro (1981) are $2\theta = 46$–$50°$, 68–73° and 88–92°. In these regions, there are six reflections of the R phase: the $(111)_R$ reflection, a reflection of the first type corresponding to the $(100)_{B2}$ reflection; $(11\bar{2})_R$ and $(300)_R$ reflections, reflections of the second type that result from splitting of the $(110)_{B2}$ reflection; the $(003)_R$ and $(22\bar{1})_R$ reflections, also reflections of the second type that appear by splitting of the $(111)_{B2}$ reflection; and a weak $(211)_R$ reflection of the third type. The agreement between the calculated and experimental peak positions and intensities is illustrated in Table 1. The refined structural parameters (Shapiro, 1981) differ slightly from (11) because the sample has a different type of dopant from our sample:

$$a^H = 7.319\,(2)\,\text{Å}, \quad c^H = 5.277\,(3)\,\text{Å},$$
$$\delta = 0.013\,(3), \quad u = 0.013\,(1), \quad v = 0.038\,(2). \quad (13)$$

Table 1 shows that the proposed structural model of the R phase agrees well with the experimental data (Shapiro, 1981). The only exception is the intensity of the $(300)_R$ reflection. Note however that $(300)_R$ and the $(11\bar{2})_R$ reflections are the components of the doublet that originates from the $(110)_{B2}$ reflection; the intensity of the parent reflection should be equally shared between the two split components. This conclusion follows not only from our theoretical analysis but also from the X-ray diffraction data (Khachin *et al.*, 1992).

Table 1. *Comparison between measured (Shapiro, 1981) and calculated (this paper) data for the R phase of* $Ti_{50}Ni_{47}Fe_3$

hkl (hexagonal setting)	$2\theta_{meas}$ (°)	$2\theta_{calc}$ (°)	I_{meas}	I_{calc}
111	48.4	48.41	1000	1000
211	68.8	68.84	12	12
$11\bar{2}$	70.4	70.36	143	134
300	71.4	71.41	230	137
003	89.0	89.01	94	129
$22\bar{1}$	91.0	91.00	397	414

Thus, we conclude that a significant difference in the measured intensities of the $(11\bar{2})_R$ and $(300)_R$ reflections found by Shapiro (1981) may be caused by the presence of preferred orientation or some similar effects and is not related to the crystal structure of the R phase.

Finally, it is necessary to discuss the experimental data presented by Hara *et al.* (1995). They present an X-ray diffraction pattern of the R phase for a Ti–50.23 at.% Ni alloy, but they present none of the numerical information that would be necessary for a detailed comparison of the calculated and measured intensity profiles. However, qualitative comparison of the experimental peak positions and reflection intensities given by Hara *et al.* (1995) and reflections from our data shows that the agreement of our theoretical model and their experimental data is quite satisfactory. For example, they consider the intensity of the 202 reflection, which agrees with experimental data only for space group $P311$ in their calculations to be one of the arguments in favor of space group $P311$ for the R phase. But the theoretical intensity of this reflection for our structural model is quite adequate to explain the experimental intensity. However, we base our model not on one reflection but on an independent theoretical analysis and comparison of our calculated results with the experimental data. That allows us to be sure of the reliability of our results.

We wish to thank the referee for a critical reading and valuable discussions.

This work was supported by the Russian Foundation for Fundamental Investigations, grant No. 97–02-16520.

References

Bührer, W., Gotthardt, R., Kulik, A. & Mercier, O. (1982). *J. Phys.* **43**(Suppl.), 219–227.

Goo, E. & Sinclair, R. (1985). *Acta Metal.* **33**, 1717–1723.

Grebennikov, V. I. & Naish, V. E. (1991). *Fiz. Met. Metalloved.* No. 4, pp. 5–18.

Hara, T., Ohba, T. & Otsuka, K. (1995). *J. Phys.* No. 5(Suppl.), pp. 641–645.

Kassan-Ogly, F. A., Kormil'tsev, E. V., Naish, V. E. & Sagaradze, I. V. (1989). *Fiz. Tverd. Tela*, **31**, 43–49.

Kassan-Ogly, F. A., Naish, V. E. & Sagaradze, I. V. (1994). *Phase Transit.* **49**, 89–141.

Khachin, V. N., Pushin, V. G. & Kondrat'ev, V. V. (1992). *Nikelid Titana: Structura i Svoistva* (*Titanium Nickelide: Structure and Properties*). Moscow: Nauka.

Lekston, Z. (1993). *Proceedings of the 15th Conference on Applied Crystallography.* Singapore: World Scientific.

Naish, V. E., Novoselova, T. V., Pushin, V. G., Sagaradze, I. V., Fedorov, V. I. & Chernenkov, Yu. P. (1996). *Phys. Met. Metallogr.* **81**, 598–606.

Naish, V. E., Novoselova, T. V. & Sagaradze, I. V. (1995). *Phys. Met. Metallogr.* **80**, 485–506.

Naish, V. E., Novoselova, T. V. & Sagaradze, I. V. (1997). *Phys. Met. Metallogr.* **84**, 18–27.

Ohba, T., Emura, Yu. & Otsuka, K. (1992). *Mater. Trans. Jpn Inst. Met.* **33**, 29–37.

Shapiro, S. M. (1981). *Metal. Trans.* **12**A, 567–573.